Time-of-Flight Implementation of an Ultra-Small-Angle Neutron Scattering Instrument

J.M. Carpenter,[ab] M. Agamalian,[a*] K.C. Littrell,[b] P. Thiyagarajan[b] and Ch. Rehm[a]

[a]Spallation Neutron Source, Oak Ridge National Laboratory, Oak Ridge, TN 37831, USA, and [b]Intense Pulsed Neutron Source, Argonne National Laboratory, Argonne, IL 60439, USA. E-mail: magamalian@anl.gov

Synopsis We present the conceptual design of a Bonse-Hart Ultra-Small-Angle Neutron Scattering (USANS) instrument, which shows that significant gains in Q-resolution and neutron flux can be achieved using multiple high-order Bragg reflections. These reflections become usable only after combining the Bonse-Hart and time-of-flight techniques.

Abstract We report calculations describing the Bonse-Hart Ultra-Small-Angle Neutron Scattering (USANS) instrument with triple-bounce Si channel-cut crystals, which show that significant gains in Q-resolution and neutron flux can be achieved using multiple high-order Bragg reflections. These reflections become usable only after combining the Bonse-Hart and time-of-flight (t-o-f) techniques, thus this variant of the USANS camera needs a pulsed neutron source. We demonstrate that t-o-f USANS instruments installed, for example, at the SNS water moderator will improve the current state of the art. Through the use of multiple wavelengths, these will provide means to detect multiple scattering effects.

Keywords: Bonse-Hart technique; Ultra-Small-Angle Neutron Scattering; time-of-flight; pulsed neutron sources

1. Introduction

The characterization of hierarchical structures spanning length scales from nanometers to microns is extremely important for materials research, polymer science, and colloidal chemistry. Systems such as nano-composites of carbon blacks in rubbers and polymers, protein hydro-gels, micro- and meso-porous materials, bones, polymers, cements, colloids, complex liquids, rocks, clays, and self-assembled fibrile structures are all examples of complex systems whose microstructures cover length scales in the range of 10 angstroms to a few microns. Conventional SANS has proven important for providing structural information on length scales in the range of 10–1000 Å. The high penetration ability of neutrons and unique contrast variation possibilities available through the use of isotope substitution make

SANS an extremely powerful technique for the studies of bulk systems with complex hierarchical structures on these length scales. However, neutron techniques that can extend these capabilities to access length scales up to several microns are much needed for materials research. USANS instruments already in place have become popular for this reason; moreover, their extension to even higher resolution, as in the time-of-flight (t-o-f) adaptation, should lead to an even broader range of applications.

Recently, the Bonse-Hart-type Ultra-SANS (USANS) Double-Crystal Diffractometer (DCD) at the High Flux Isotope Reactor (HFIR) at the Oak Ridge National Laboratory (ORNL) has been modified to prevent contamination of the rocking curve wings by single-bounce back-face reflections, end-face reflections, and surface-induced scattering (Agamalian *et al.*, 1997; Agamalian *et al.*, 1998). This breakthrough resulted in an improvement of the signal-to-noise ratio (SNR) by more than three orders of magnitude. This new instrument has added nearly two orders of magnitude (2×10^{-5} Å^{-1} < Q < 10^{-3} Å^{-1}, $Q = 4\pi\sin\theta/\lambda$, where 2θ is the scattering angle and λ is the neutron wavelength) to the range of length scales accessible to neutron scattering investigations, and presently represents the state of the art for this class of instruments. More than twenty scientific groups from domestic and foreign institutions have used the ORNL USANS instrument, producing several significant scientific advances in petrology (Radlinski *et al.*, 1999) and polymer science (Agamalian *et al.*, 2000). One of the discoveries made using the HFIR USANS instrument was the observation of surface fractal structure of extremely long extent in sedimentary rocks (Radlinski *et al.*, 1999). New USANS instruments at the reactor of the National Institute for Science and Technology (NIST), in Europe, and Japan incorporate the new concepts developed at ORNL.

About 50% of the materials problems that SANS addresses in a wide range of scientific disciplines require data covering length scales larger than accessed in conventional SANS, which the USANS technique provides. Currently, the USANS technique can extend the range of Qs down to ~ 2×10^{-5} Å^{-1}, which corresponds to the distance of ~ 30 μm in real space. The further extension of this limit will enable examination of even larger inhomogeneities. Substantial intensity loss inhibits such extensions of reactor-based instruments using the single-wavelength mode. However, the t-o-f implementation of USANS conveniently provides this extension. In addition, the multi-wavelength instrument opens the opportunity for immediate detection of multiple scattering without requiring testing of samples of different thickness. These two novel features will move the USANS technique into new regimes of science. The high-intensity pulsed neutron sources such as SNS will make this possible.

We are developing conceptual designs for t-o-f USANS instruments that allow the measurement of SANS data in the range of length scale from 1000 Å to 200 μm for the

structural characterization of materials. The ultimate goal is to provide for the construction of t-o-f USANS instruments at SNS. We consider below two different configurations of the t-o-f USANS camera, one optimized for the highest flux while preserving the conventional USANS Q-resolution, and the other optimized for the highest Q resolution while preserving flux.

2. Basic concepts of a t-o-f USANS instrument

We describe here two aspects of the t-o-f USANS principle. The first novelty of this concept is that neutrons with multiple harmonic wavelengths are distinguished using t-o-f techniques: Neutrons with a series of different wavelengths satisfying Bragg's law, $n\lambda_n = 2d\sin\Theta_B$, where d is the lattice spacing between a given set of crystal planes and n = 1, 2, 3, … is the order of diffraction, are scattered at the same Bragg angle Θ_B. Because the neutron speed v is inversely proportional to its wavelength, the time-of-arrival L/v is proportional to the wavelength, where L is the distance from the source to the detector. The corresponding diffracted neutrons (see Fig. 1) arrive at the detector at different times, well resolved because of the short source pulses. This provides simultaneous parallel measurement of the USANS signal: Using, say, up to eight different wavelengths leads to significant intensity enhancement compared to using the monochromatic reactor-based USANS instruments. Meanwhile t-o-f separation of orders of Bragg reflection obviates the problem of harmonic contamination that occurs in instruments with steady beams.

Moreover, what is the second significant aspect of the t-o-f instrument is that because the angular resolution (the rocking curve width) DCD is proportional to λ_n^2 (also see Fig. 1), the use of the high-order diffraction peaks, $\lambda_n = \lambda_1/n$, i.e., λ_1, $\lambda_1/2$, $\lambda_1/3$, $\lambda_1/4$, etc., allows the achievement of significantly higher Q-resolution than the use of only one low-order reflection.

According to the Darwin theory, changing the Bragg angle Θ_B also alters the angular resolution. Because the reflectivity function of a perfect transparent crystal (valid for Si described here) to a first approximation has a rectangular shape, only one parameter, its Darwin Plateau (DP), $2\delta\theta_n$, is necessary for its characterization. The full width of the DP is

$$2\delta\theta_n = [2|F(n)|/\pi V_0]\cdot[(\lambda_1/n)^2/\sin 2\Theta_B] \quad (1)$$

where V_0 is the volume of the crystallographic unit cell, and $|F(n)|$ is the magnitude of the structure factor of Si, which is the same for all orders of the (220) reflection but which oscillates with order number n as $(1-\sin(\pi n/2))$ for the (111) family of reflections. The intensity reflected from a perfect crystal oriented at the Bragg angle within the Darwin

plateau is usually very close to unity. This statement is valid not only for the first-order reflection, but also for its higher harmonics as shown in Fig. 1. It is worthwhile to note that the first factor in formula (1) depends only on the parameters of a chosen crystal, thus the DP, $2\delta\theta_n$, scales as $(\lambda_1/n)^2 /\sin 2\Theta_B = 4d^2 \tan\Theta_B/n^2$. Figure 2 shows that the DP of the first-order reflection calculated for Si(111) and Si(220) increases significantly in the range $20° < \Theta_B < 88°$ as the Bragg angle increases. The distinction between our conceptual designs for t-o-f USANS instruments optimized for the highest flux and for highest resolution rests on the basis of this ability to separately choose the angular resolution and the wavelength of diffraction peaks, λ_1, $\lambda_1/2$, $\lambda_1/3$, $\lambda_1/4$, etc. by changing the Bragg angle and the d-spacing of the Si channel-cut crystals.

The scattering vector $Q = 4\pi\sin(\Theta)/\lambda$, where Θ is one-half the scattering angle, is the main parameter of any SANS experiment; conventionally, its minimal value, Q_{min}, quantifies the Q-resolution, ΔQ, for many types of the SANS instruments. The Bonse-Hart t-o-f USANS instrument is one such an instrument; ΔQ_n is conveniently connected to the value of DP through the relation

$$\Delta Q_n = Q_{min}(n) = 4\pi\sin[\delta\theta_n]/\lambda_n \approx 4\pi\delta\theta_n/\lambda_n = [4F(n)/V_0]\cdot[(\lambda_1/n)/\sin 2\Theta_B] \qquad (2)$$

Equation (2) clearly shows that $\Delta Q_n \propto \lambda_1/n$. Thus the resolution of a t-o-f USANS instrument increases significantly when the high-order Bragg reflections are used.

3. t-o-f USANS optimized for the highest flux and the highest resolution

At the SNS, the H_2O poisoned, decoupled moderator provides the highest flux of thermal neutrons in the intermediate range of wavelengths. We choose that moderator as the basis for our example assessments. The optimal flux in the range $0.5 \text{ Å} < \lambda < 2.0 \text{ Å}$ can be achieved by increasing the density of the Bragg reflections in this interval (see Fig. 3). It is important to maintain $Q_{min} \approx 2\times10^{-5} \text{ Å}^{-1}$, which corresponds to Q-resolution of the reactor-based USANS instruments. Fig. 1 clearly indicates that the density of high-order Bragg reflections is increased with the increase of n. Therefore, the number of reflections in the range of wavelengths of interest, $0.5 \text{ Å} < \lambda < 2.0 \text{ Å}$, will be increased when the first-order peak is shifted to higher values of λ. The latter, according to the Bragg formula, can be done by increasing Θ_B, which, however, also leads to an increase of DP (see Fig. 2).

Figure 4 shows a discrete spectrum of the neutron flux Bragg-reflected from a Si(111) crystal oriented at $\Theta_B = 75°$. The peaks, $\lambda_1/3,\ldots, \lambda_1/12$, are located in the range of wavelength, $0.5 \text{ Å} < \lambda < 2 \text{ Å}$, however, the first-order reflection at $\lambda_1 \approx 6$ Å has relatively low peak

intensity. Thus, in spite of a rather broad DP (≈ 14 arcsec, see Table 1), its contribution to the total t-o-f USANS flux summarized over all reflections shown in Fig. 4 seems to be insignificant. It is reasonable to abandon this peak, as this decreases the upper cut-off of the operating bandwidth from $\lambda \approx 6.0$ Å to $\lambda = 2.0$ Å (see Fig. 3), and eliminates a possible time-frame overlapping problem almost without cost in either intensity or data quality. Thus, the high-flux USANS instrument based on triple-bounce Si(111) channel-cut crystals permits parallel measurements of eight scattering curves per one angular scan using $\lambda_1/3$, $\lambda_1/4$, $\lambda_1/5$, $\lambda_1/7$, $\lambda_1/8$, $\lambda_1/9$, $\lambda_1/11$, $\lambda_1/12$ monochromatic lines (see Fig. 4). The Q-resolution of the t-o-f USANS [see equation (2)] is higher for the high-order reflections because the DP decreases as λ^2, as shown qualitatively in Fig. 2. As a result, one of the most important parameters, Q_{min}, varies from $Q_{min} \approx 2.5\times10^{-5}$ Å^{-1} for the $\lambda_1/3$ reflection to $Q_{min} \approx 1\times10^{-5}$ Å^{-1} for the $\lambda_1/12$ reflection. Therefore, the best Q-resolution of this setting is equal to or even slightly better than that of the corresponding reactor-based USANS cameras. Fig. 4 gives us only a qualitative picture of the high-order reflections distribution; the actual flux at the sample position has been determined (see the following paragraph 4) from the Monte Carlo simulation of the SNS t-o-f USANS instrument by taking into consideration the source brightness and the contribution of the optical components. Figure 5 shows an optical scheme of the high-flux t-o-f USANS camera with triple-bounce Si(111) channel-cut crystals (Fig. 6a) designed for the Bragg angle $\Theta_B = 75°$. In this design the reflected beam is 5 cm tall and 3 cm wide, which is similar to that for the NIST USANS camera (http://www.ncnr.nist.gov/instruments/usans). The layout in Fig. 5 does not include the upstream optical elements, a neutron guide, and a pre-monochromator.

The high-resolution t-o-f USANS instrument is also optimized for the same SNS H_2O poisoned, decoupled moderator choosing Si(220) crystal set up at the Bragg angle, $\Theta_B = 50^o$. This configuration allows use of six Bragg peaks (see Fig. 7) in the wavelength range, 0.49 Å $< \lambda <$ 3 Å, with the best value of $Q_{min} = 4\times10^{-6}$ Å^{-1}. This Q-resolution is five times higher than that for the best present reactor-based Bonse-Hart USANS instrument. The main crystallographic and diffraction parameters for the high-resolution configuration of the t-o-f USANS are listed in Tab. 1; its optical scheme is similar to that shown in Fig. 5. The channel-cut crystals (Fig. 6b) designed for the Bragg angle $\Theta_B = 50°$ also allow to reflect a neutron beam with the cross-section area 5 cm × 3 cm.

These two configurations of the t-o-f USANS instrument described here represent a novel approach to extending the range and usefulness of the Bonse-Hart USANS technique.

4. Monte Carlo simulations of the SNS t-o-f USANS instrument

The expected neutron intensities for these two configurations of the t-o-f USANS instrument were calculated using IDEAS, a Monte Carlo simulation package for neutron scattering instrumentation (Lee *et al.*, 2001). Given a moderator emission profile, IDEAS calculates the characteristics of a neutron beam through the instrument. The setup for the t-o-f USANS calculations (see Fig. 8) starts with a module representing the SNS bottom upstream decoupled, asymmetrically-poisoned water moderator (width: 10 cm, height: 12 cm). The emitted neutrons are channeled through a 12.7-m-long guide starting 2.3 m from the moderator. To study potential enhancements in neutron flux, which can be obtained by using the neutron guides with supermirror coating, the guide module was parameterized with non-reflecting walls as well as with supermirror-coated walls (of m = 3 quality). The double-crystal arrangement (cf. Fig. 5) has been substituted in this simulation with one single-bounce crystal plate, which reflects the fact that the peak intensity of a neutron beam reflected from a perfect crystal at the exact Bragg position does not change significantly after multiple reflections. For a given Bragg angle, the distance A between guide and reflecting crystal was chosen to be as small as possible while allowing the detector a full view of the diffracting surface. Detector modules, recording the intensity of the scattered neutrons as a function of wavelength, were placed a few centimeters, B, and 3 m, B', downstream from the "crystal," respectively to examine the intensity lost due to the beam divergence. Representing the channel-cut crystal as a single-bounce plate is a convenience that has almost no effect on the result. Table 2 summarizes the parameters for our simulation of the neutron flux for the high-flux [Si(111), $\Theta_B = 75°$], and the high-resolution [Si(220), $\Theta_B = 50°$] configuration of the t-o-f USANS instrument; the distances are those defined in Fig. 8.

Fig. 9 shows the neutron fluxes in [n/cm^2/sec] calculated separately for each order of reflection of the high-flux configuration at the distances 0.2 m (a) and 3 m (b). The fluxes for each order of reflection are integrated over the corresponding Bragg peak calculated as a function of wavelength. The overall fluxes, calculated as a sum of all Bragg peaks for a chosen distance and coating, are also given in figures 9(a) and 9(b). Figure 10 gives the similar information for the high-resolution configuration of the t-o-f USANS instrument. Figures 9 and 10 clearly show a significant (approximately 3 times) increase of the overall flux after adding the neutron guides with the supermirror coating. The calculated fluxes are comparable to the neutron flux of the NIST USANS instrument, which is ~ 3000 n/cm^{2}sec.

5. Summary and conclusions

The present calculations clearly show the following advantages of the multi-order t-o-f USANS instrument:

- The flux gain factor related to the multi-wavelength performance makes the t-o-f USANS flux comparable with that for the best existing reactor-based USANS instruments.
- The high-resolution setup dramatically extends the value of Q_{min}, from 2×10^{-5} Å^{-1} to ~ 4×10^{-6} Å^{-1}, which will allow measurements of enormously large inhomogeneities with dimensions up to 200 μm.
- Parallel measurements at different wavelengths will be helpful for diagnosing multiple scattering in the USANS experiments, which is very common for this dynamical range of neutron diffraction.

The presented calculations are based on an ideal theoretical model ignoring for example the effect of the Debye-Waller factor on the reflectivity distribution, and a more realistic approach is in progress.

Figure captions

Figure 1 Diffraction peaks Bragg-reflected from a perfect crystal oriented at a fixed angle with respect to the "white" primary beam, or to the pre-monochromator made with the same crystal cut parallel to the same crystallographic plane.

Figure 2 Angular dependence of the Darwin Plateau calculated for Si(111) and Si(220).

Figure 3 Neutron flux originated by the SNS H_2O poisoned, decoupled moderator and the bandwidth, 0.5 Å < λ < 2.0 Å, chosen for the high-flux version of t-o-f USANS.

Figure 4 Spectrum of Bragg reflections from Si(111) crystal set up at $\Theta_B = 75°$.

Figure 5 Optical scheme of the high-flux t-o-f USANS instrument with triple-bounce Si(111) crystals designed for the Bragg angle $\Theta_B = 75°$.

Figure 6 The design of triple-bounce channel-cut crystals (top view) for the 3 cm wide neutron beam: (a) Si(111) for $\Theta_B = 75°$; (b) Si(220) for $\Theta_B = 50°$.

Figure 7 Spectrum of Bragg reflections from Si(220) crystal set up at $\Theta_B = 50°$.

Figure 8 Setup for t-o-f USANS Monte Carlo simulations.

Figure 9 Monte Carlo-determined fluxes at the distances B (a) and B' (b) for the high-flux configuration of the t-o-f USANS instrument placed at the end of the neutron guide with $m = 3$ supermirror coating (filled circles), and with non-reflecting walls (open circles).

Figure 10 Monte Carlo-determined fluxes at the distances *B* (a) and *B′* (b) for the high-resolution configuration of the t-o-f USANS instrument placed at the end of the neutron guide with $m = 3$ supermirror coating (filled circles), and with non-reflecting walls (open circles).

Table 1 Bragg diffraction parameters for Si(111) and Si(220) useful for t-o-f USANS.

Crystal (h, k, l)	a, cell edge [Å]	d-spacing [Å]	F, 10^{-4} [Å]	λ_1 [Å]	Θ_B [deg]	Darwin width 2δθ [arcsec]	Missed orders
Si(111)	5.431	3.1355	2.316	6.057	75	13.931	$\lambda_1/2$, $\lambda_1/6$, $\lambda_1/10$
Si(220)	5.431	1.9201	3.203	2.942	50	2.3072	none

Table 2 Parameters for calculations of the high-flux and high-resolution configurations.

Perfect Crystal	Si(111)	Si(220)
Θ_B	75°	50°
Distance *A*	0.19 m	0.06 m
Distance *B*	0.2 m	0.10 m
Distance *B′*	3 m	3.0 m

References

Agamalian, M., Alamo, R.G., Londono, J.D., Mandelkern, L. & Wignall, G.D. (2000). *J. Appl. Cryst.* **33**, 843-846.

Agamalian, M., Christen, D.K., Drews, A.R., Glinka, C.J., Matsuoka, H. & Wignall, G.D. (1998). *J. Appl. Cryst.* **31**, 235-240.

Agamalian, M., Wignall, G.D. & Triolo, R. (1997). *J. Appl. Cryst*. **30**, 345-352.

http://www.ncnr.nist.gov/instruments/usans, Perfect Crystal Diffractometer (PCD) for Ultra-High Resolution Small-Angle Neutron Scattering.

Lee, W.T., Wang, X.L., Robertson, J.L., Klose, F. & Rehm, Ch. (2002). *Appl. Phys. A*. In the press.

Radlinski, A.P., Radlinska, E.Z., Agamalian, M., Wignall, G.D., Lindner, P. & Randl, O.G. (1999). *Phys. Rev. Lett.* **82**, 3078-3081. See also *Physical Review Letters Focus*, http://focus.aps.org/v3/st22.html.

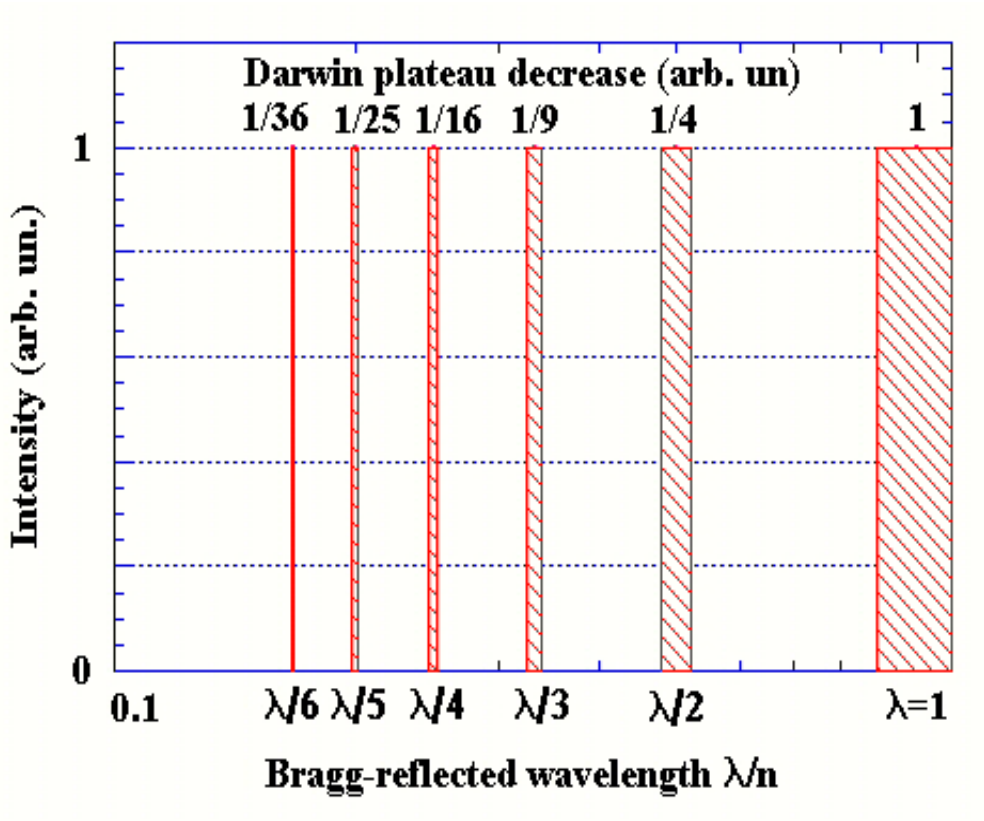
Darwin plateau decrease (arb. un)
1/36
1/25
1/16
1/9
1/4
1
1
0
Intensity (arb. un.)
0.1
λ/6
λ/5
λ/4
λ/3
λ/2
λ=1
Bragg-reflected wavelength λ/n

Fig. 1

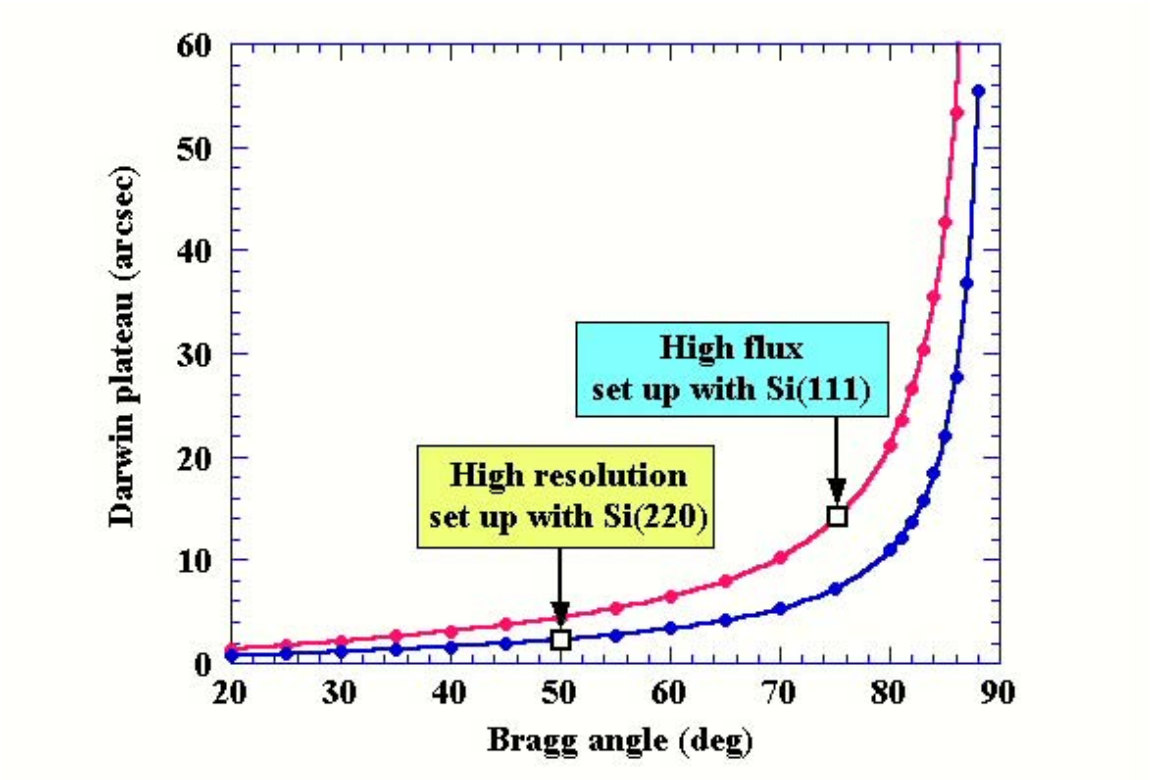
Darwin plateau (arcsec)
Bragg angle (deg)
High flux
set up with Si(111)
High resolution
set up with Si(220)
0
10
20
30
40
50
60
20
30
40
50
60
70
80
90

Fig. 2

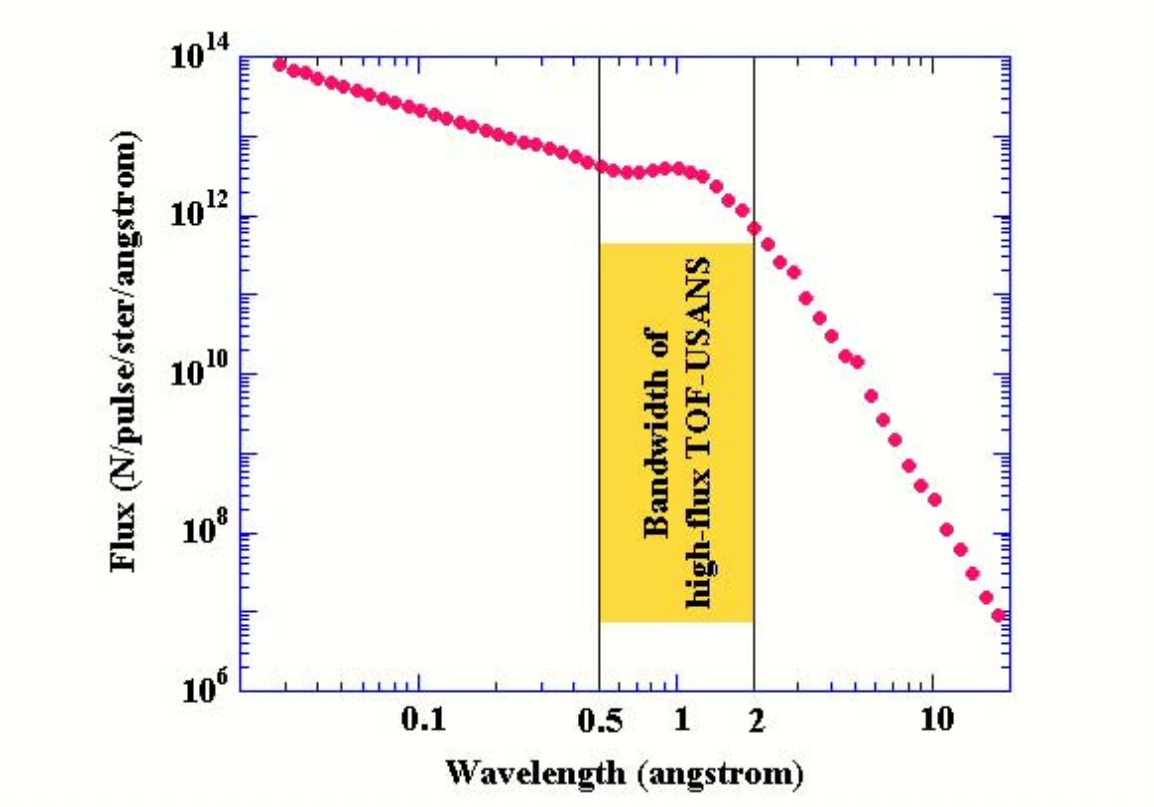
Flux (N/pulse/ster/angstrom)
10^{14}
10^{12}
10^{10}
10^{8}
10^{6}
Bandwidth of
high-flux TOF-USANS
0.1
0.5
1
2
10
Wavelength (angstrom)

Fig. 3

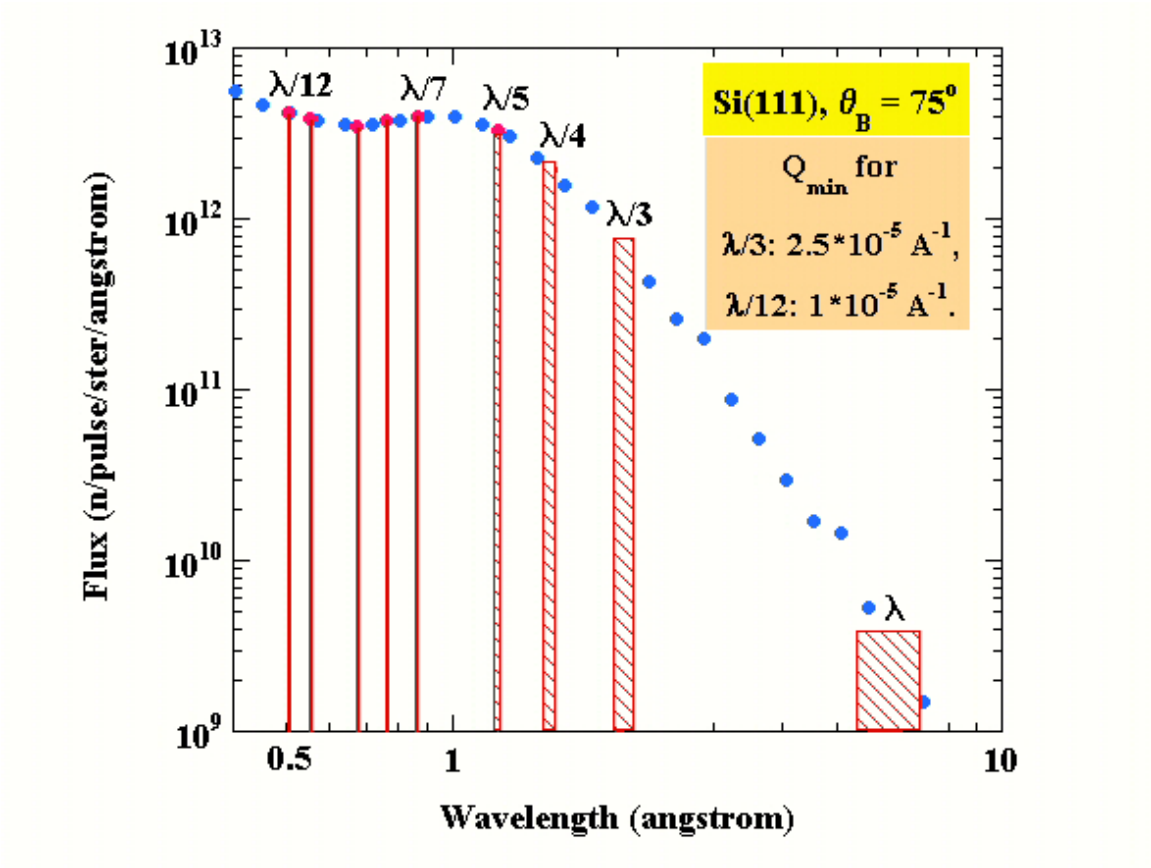
Flux (n/pulse/ster/angstrom)
Wavelength (angstrom)
λ/12
λ/7
λ/5
λ/4
λ/3
λ
Si(111), θB = 75°
Qmin for
λ/3: 2.5*10-5 A-1,
λ/12: 1*10-5 A-1.

Fig. 4

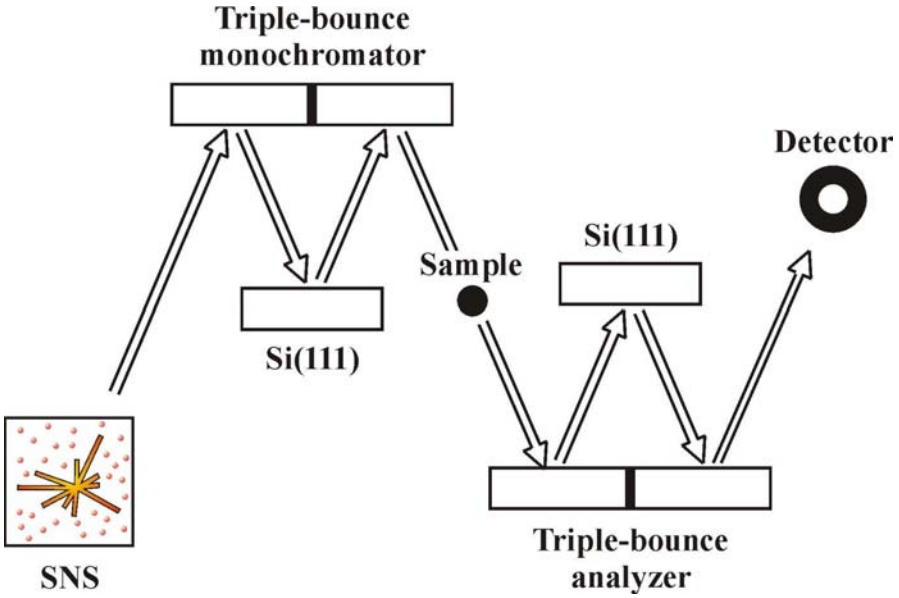
Triple-bounce
monochromator
Detector
Si(111)
Sample
Si(111)
SNS
Triple-bounce
analyzer

Fig. 5

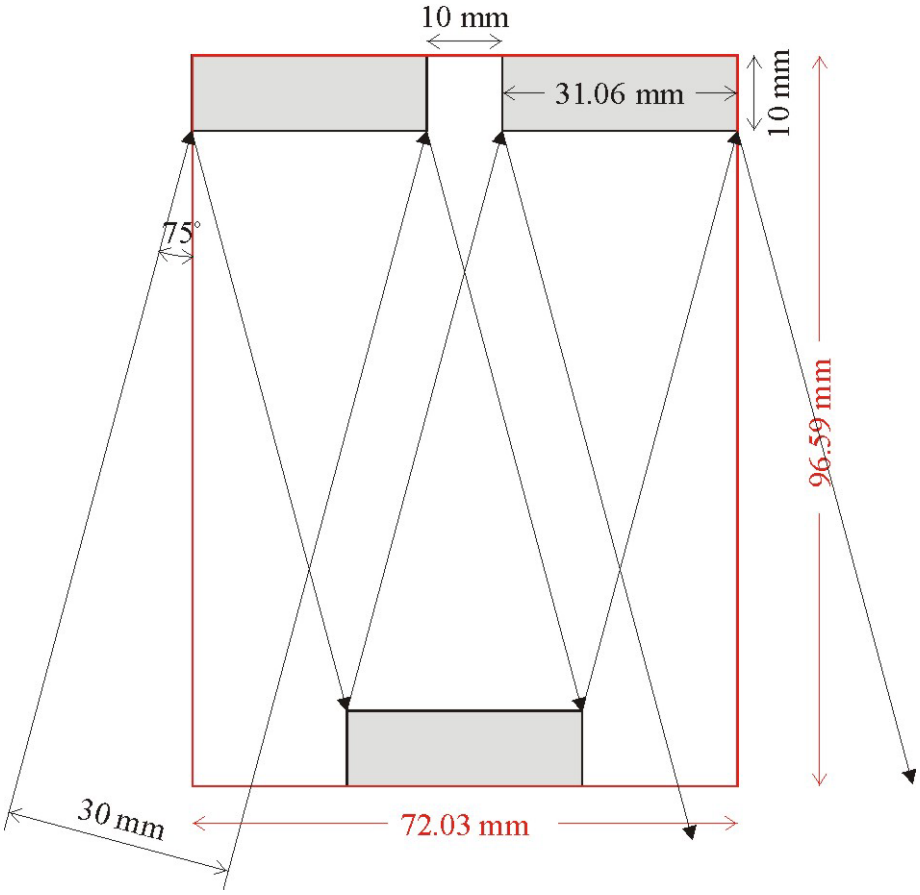
10 mm
31.06 mm
10 mm
75°
96.59 mm
30 mm
72.03 mm

(a)

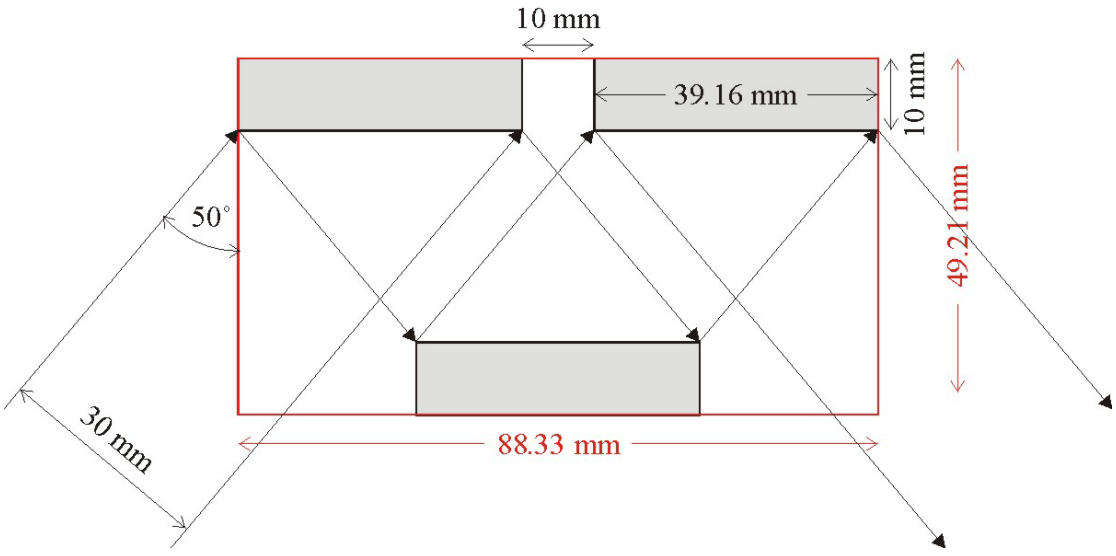
10 mm
39.16 mm
10 mm
50°
49.21 mm
30 mm
88.33 mm

(b)

Fig. 6

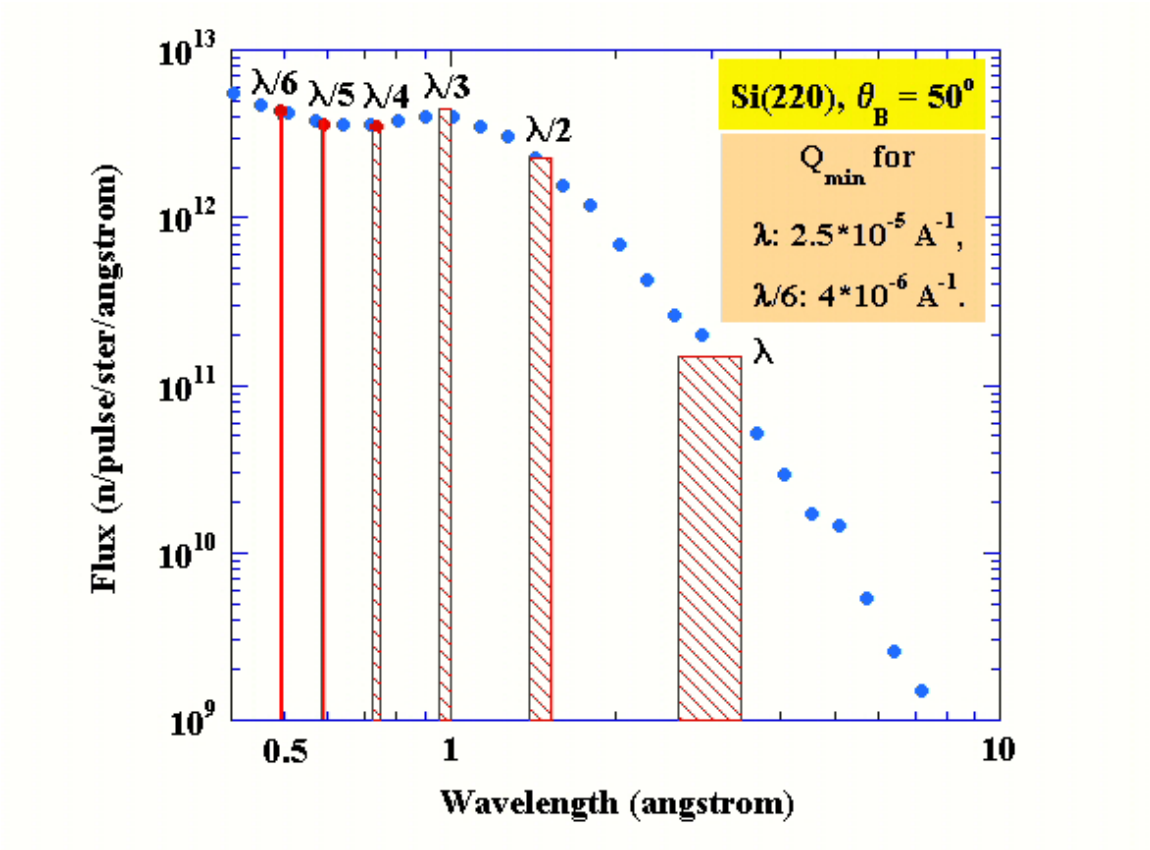
Flux (n/pulse/ster/angstrom)
Wavelength (angstrom)
λ/6
λ/5
λ/4
λ/3
λ/2
λ
Si(220), θB = 50°
Qmin for
λ: 2.5*10-5 A-1,
λ/6: 4*10-6 A-1.

Fig. 7

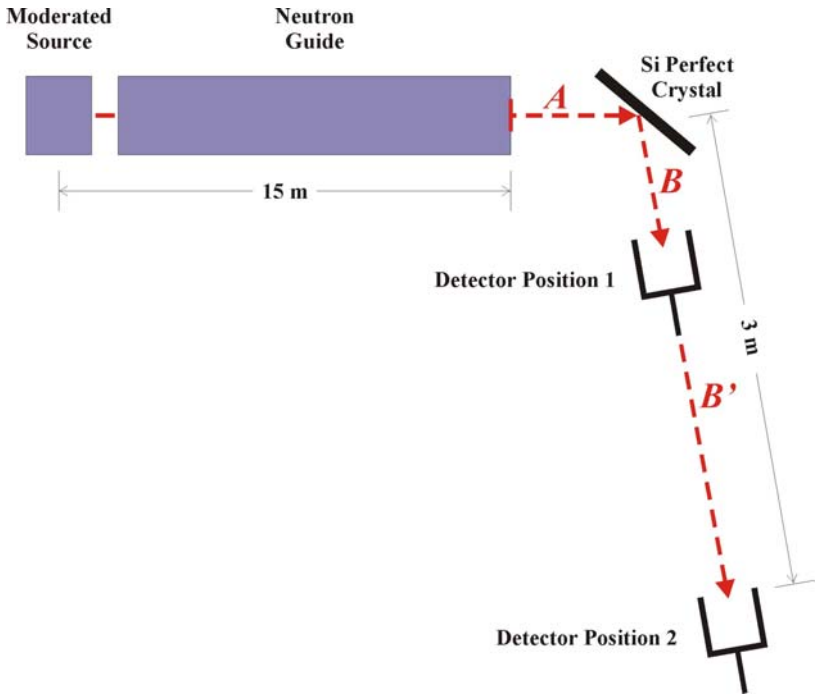
Moderated
Source
Neutron
Guide
Si Perfect
Crystal
A
B
15 m
Detector Position 1
3 m
B'
Detector Position 2

Fig. 8

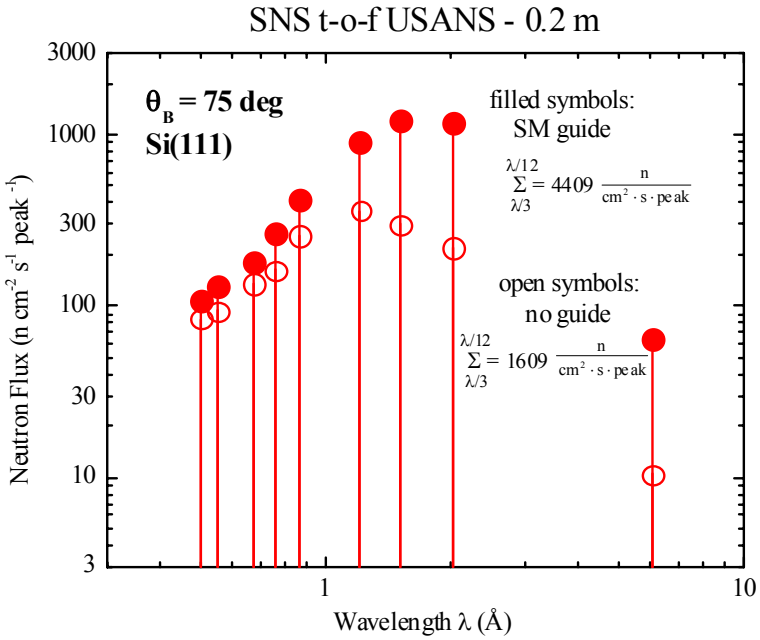
SNS t-o-f USANS - 0.2 m
θB = 75 deg
Si(111)
filled symbols:
SM guide
Σ λ/12 λ/3 = 4409 n / cm² · s · peak
open symbols:
no guide
Σ λ/12 λ/3 = 1609 n / cm² · s · peak
Neutron Flux (n cm⁻² s⁻¹ peak⁻¹)
3000
1000
300
100
30
10
3
1
10
Wavelength λ (Å)

(a)

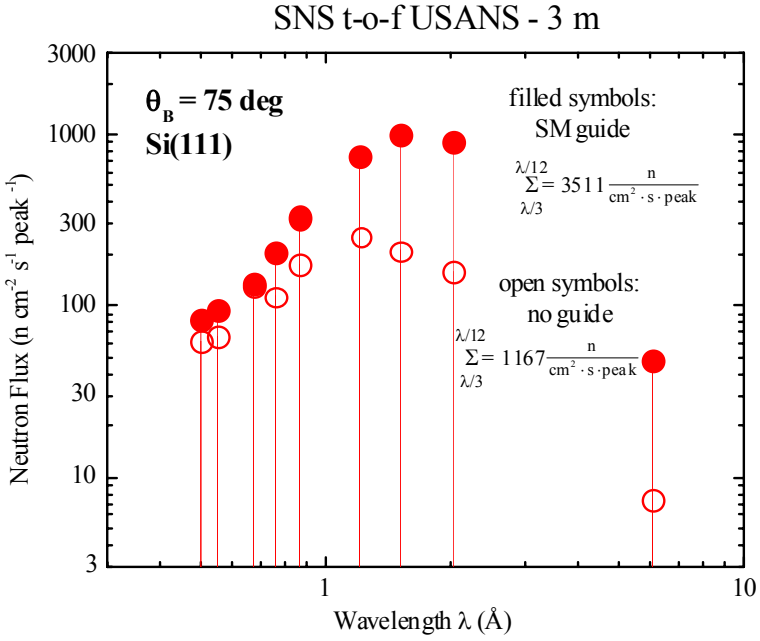
SNS t-o-f USANS - 3 m
θB = 75 deg
Si(111)
filled symbols:
SM guide
Σ λ/12 λ/3 = 3511 n / cm² · s · peak
open symbols:
no guide
Σ λ/12 λ/3 = 1167 n / cm² · s · peak
Neutron Flux (n cm⁻² s⁻¹ peak⁻¹)
3000
1000
300
100
30
10
3
1
10
Wavelength λ (Å)

(b)

Fig. 9

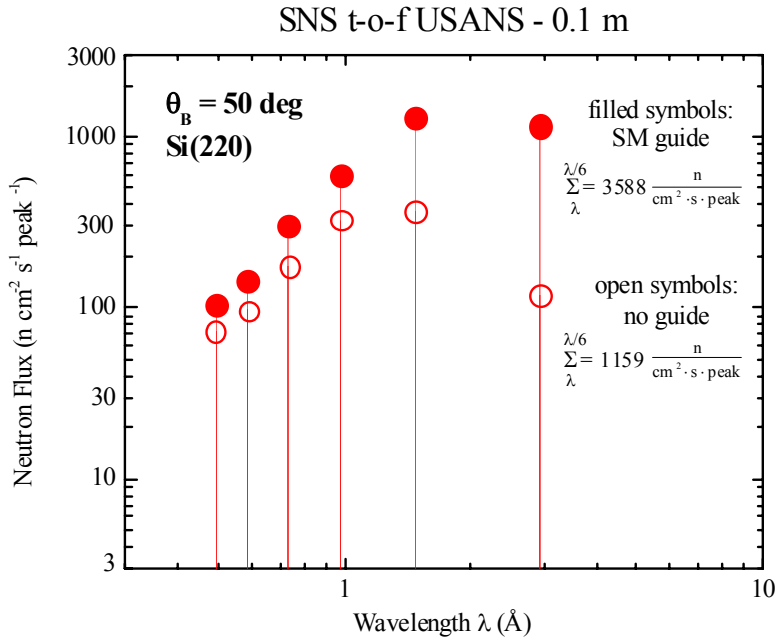
SNS t-o-f USANS - 0.1 m
θB = 50 deg
Si(220)
filled symbols:
SM guide
Σ λ/6 λ = 3588 n / cm² · s · peak
open symbols:
no guide
Σ λ/6 λ = 1159 n / cm² · s · peak
Neutron Flux (n cm⁻² s⁻¹ peak⁻¹)
Wavelength λ (Å)
3000
1000
300
100
30
10
3
1
10

(a)

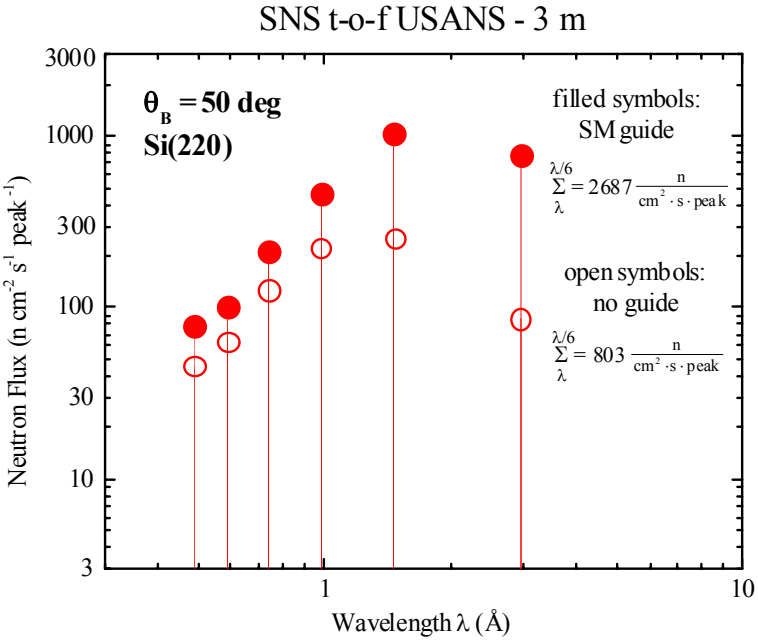
SNS t-o-f USANS - 3 m
θB = 50 deg
Si(220)
filled symbols:
SM guide
Σ λ/6 λ = 2687 n / cm² · s · peak
open symbols:
no guide
Σ λ/6 λ = 803 n / cm² · s · peak
Neutron Flux (n cm⁻² s⁻¹ peak⁻¹)
Wavelength λ (Å)
3000
1000
300
100
30
10
3
1
10

(b)

Fig. 10